Liquid Crystals

ISSN: (Print) (Online) Journal homepage: https://www.tandfonline.com/loi/tlct20

Ideal mixing of paraelectric and ferroelectric nematic phases in liquid crystals of distinct molecular species

Xi Chen, Zhecong Zhu, Mitchell J. Magrini, Eva Korblova, Cheol S. Park, Matthew A. Glaser, Joseph E. Maclennan, David M. Walba & Noel A. Clark

To cite this article: Xi Chen, Zhecong Zhu, Mitchell J. Magrini, Eva Korblova, Cheol S. Park, Matthew A. Glaser, Joseph E. Maclennan, David M. Walba & Noel A. Clark (2022) Ideal mixing of paraelectric and ferroelectric nematic phases in liquid crystals of distinct molecular species, Liquid Crystals, 49:11, 1531-1544, DOI: 10.1080/02678292.2022.2058101

To link to this article: https://doi.org/10.1080/02678292.2022.2058101

LIQUID CRYSTALS
2022, VOL. 49, NO. 11, 1531–1544
https://doi.org/10.1080/02678292.2022.2058101

Taylor & Francis
Taylor & Francis Group

Ideal mixing of paraelectric and ferroelectric nematic phases in liquid crystals of distinct molecular species

Xi Chen [a], Zhecong Zhu [a], Mitchell J. Magrini [b], Eva Korblova [b], Cheol S. Park [a], Matthew A. Glaser [a], Joseph E. Maclennan [a], David M. Walba [b] and Noel A. Clark [a]

[a]Department of Physics and Soft Materials Research Center, University of Colorado, Boulder, CO, USA; [b]Department of Chemistry and Soft Materials Research Center, University of Colorado, Boulder, CO, USA

ABSTRACT

The organic mesogens RM734 and DIO are members of separate molecular families featuring distinct molecular structures. These families are the first ones known to exhibit a ferroelectric nematic liquid crystal phase. Here, we present an experimental investigation of the phase diagram and electro-optics of binary mixtures of RM734 and DIO. We observe paraelectric nematic and ferroelectric nematic phases in both materials, each of which exhibits complete miscibility across the phase diagram, showing that the paraelectric and ferroelectric are the same phases in RM734 and DIO. Remarkably, these molecules form ideal mixtures with respect to both the paraelectric–ferroelectric nematic phase behaviour and the ferroelectric polarisation density of the mixtures, the principal order parameter of the transition. Ideal mixing is also manifested in the orientational viscosity, and the onset of glassy dynamics at low temperature. This behaviour is attributable in part to the similarity of their overall molecular shape and net longitudinal dipole moment, and to a common tendency for head-to-tail molecular association. In contrast, the significant difference in molecular structures leads to poor solubility in the crystal phases, enhancing the stability of the ferroelectric nematic phase at low temperature in the mixtures and enabling room-temperature electro-optic effects.

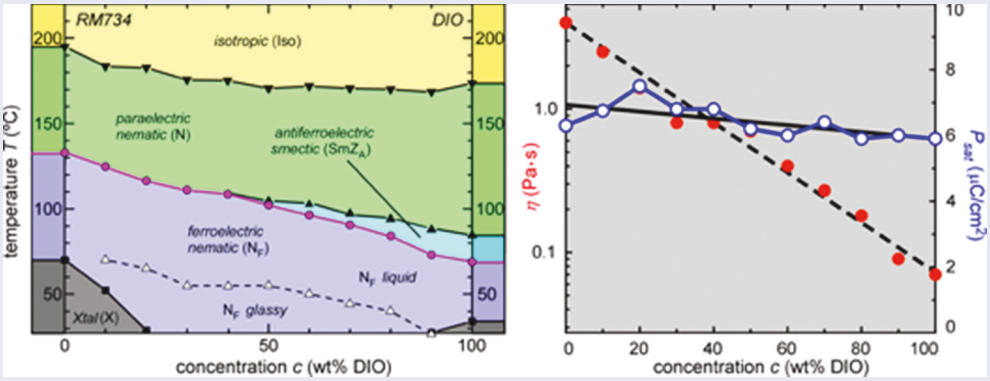

ARTICLE HISTORY
Received 30 October 2021
Accepted 22 March 2022

KEYWORDS
Liquid crystal; ferroelectric nematic; polar liquid; phase behavior; ideal mixing

Introduction

Ferroelectricity in liquids was predicted in the 1910s by P. Debye [1] and M. Born [2], who applied the Langevin-Weiss model of ferromagnetism to the orientational ordering of molecular electric dipoles. A century later, in 2017, two groups independently reported novel nematic phases of polar molecules, the antiferroelectric splay nematic in the molecule RM734 [3–5] and a 'ferroelectric-like' phase in the molecule DIO [6]. Ferroelectricity has subsequently been demonstrated in RM734 [7] and in DIO, as confirmed in our own experiments and by Li et al. [8]. The serendipity of this development is remarkable since, as is evident from Figure 1, RM734 and DIO are members of separate molecular families with distinctly different molecular structures. Novel polar nematics have been independently observed in close homologs and mixtures within these families

CONTACT Joseph E. Maclennan jem@colorado.edu

This article has been corrected with minor changes. These changes do not impact the academic content of the article.

Supplemental data for this article can be accessed here

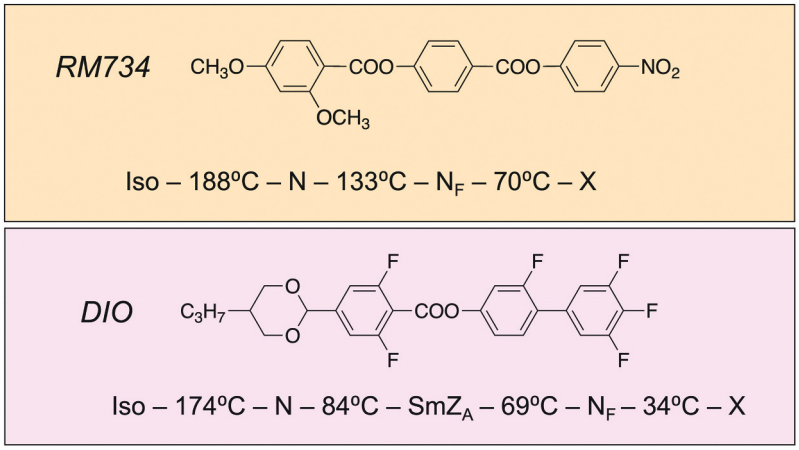

Figure 1. (Colour online) RM734 and DIO are representative members of nitro- and fluoro-based molecular families that exhibit novel polar nematic phases. Ferroelectric nematics (N_F) have been observed independently in both materials, and in close homologs within each family. DIO exhibits, in addition, an intermediate phase, the SmZ_A, recently shown to be an antiferroelectric smectic.

[3,8–12]. On the other hand, DIO and RM734 have similar molecular shape and size, and both molecules have longitudinal molecular dipole moments of ~ 11 Debye, similarities which could favour their miscibility in an N_F phase.

These observations motivated us to pursue the study of the interactions between these distinct molecular species in the context of nematic ferroelectricity. Here, we present an experimental investigation of the phase and electro-optic behaviour of binary DIO/RM734 mixtures. Similarities in the optical textures, calorimetry, and second-harmonic generation of RM734 and DIO were recently reported by Li et al. [8], but the question of whether the ferroelectric nematics identified in RM734 and DIO are the same phase can be answered unambiguously only by investigating binary miscibility [13]. The phenomenology of mixing these materials in their ferroelectric nematic phases was unknown, but, because of their chemical differences, it appeared unlikely that these molecules would be very miscible in their crystal phases, promising an opportunity to suppress crystallisation and achieve room-temperature, ferroelectric mixtures. In relation to this study, we also investigated the M2 phase originally reported in DIO [6] but not structurally characterised. Synchrotron-based microbeam small-angle x-ray scattering (SAXS) and electro-optic polarised light microscopy show the M2 to be a lamellar, density-modulated antiferroelectric LC having a nematic director parallel to the layer planes, a phase which we term Smectic Z (SmZ_A) in work reported elsewhere [14].

Nematic ferroelectricity presents opportunities for novel liquid crystal science and technology thanks to its unique combination of macroscopic polar ordering and fluidity. The ferroelectric nematic (N_F) phase of RM734 shows a rapid electro-optic response at high temperature in the N_F range [15] but exhibits crystallisation and a viscosity that grows strongly on slow cooling. The room temperature N_F phase that is obtained by quenching, on the other hand, is glassy. In the applications development of liquid crystal technologies, the exploration of mixtures is a time-honoured and highly successful approach to addressing issues such as eliminating crystallisation [16], expanding phase ranges [17], and tuning liquid crystal properties [18]. Studies of mixtures are also key to advancing liquid crystal science, providing a way to test structural models of phases by continuously varying the composition [19], to find phases in mixtures that are not exhibited by any of their components [20,21], and to discover new phases [22].

Results

Phase diagram

RM734 and DIO were synthesised using, respectively, the schemes published in [7] and shown in Fig. S1. The phase diagram for different weight percent (wt %) of DIO in the mixture, *c*, determined upon slow cooling (at −1K/min) from the isotropic (Iso) phase using polarised light microscopy (PLM) in transmission, differential scanning calorimetry (DSC), polarisation measurement, and SAXS experiments, is shown in Figure 2. A well-defined phase front passing through the cell was observed in the microscope at each of the transitions, allowing an accurate determination of the transition temperatures. The observed transition temperatures of the neat

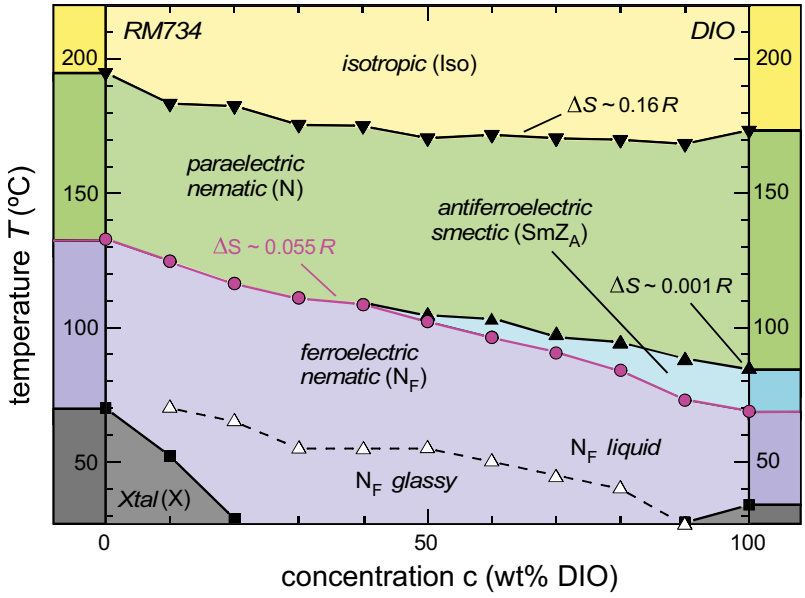

Figure 2. (Colour online) Phase diagram of the RM734 and DIO binary mixture upon cooling. The phase transition temperatures were determined using polarized light microscopy, DSC, and polarisation current measurements. Continuous miscibility within the Iso, N, and N_F phases indicates that they are the same phases in RM734 and DIO. The transitions are first-order, with average entropy changes across the phase diagram of: ▼ – $\Delta S \sim (0.16 \pm 0.01)R$; ● – $\Delta S \sim (0.055 \pm 0.01)R$. The N – SmZ_A transition is very weakly first-order (▲ $-\Delta S \sim 0.001R$ for DIO [6]). The temperature of the transition to the N_F phase (magenta circles) varies approximately linearly with concentration, indicating ideal mixing behaviour of RM734 and DIO, and equal entropy changes $\Delta S_{DIO} = \Delta S_{RM734}$ at this transition. The SmZ_A phase of DIO, which is not observed for $c < 40$ wt%, has been identified as an antiferroelectric smectic [14]. This phase is lamellar and density-modulated, with the director parallel to the plane of the layers, and the polarization alternating in sign from layer to layer. The effective orientational viscosity of the mixtures, η, increases rapidly on cooling, reaching ~5 Pa·s at the dashed line, heralding the approach to an orientational glass transition. Crystallization is not observed in the glass but occurs at either end of the phase diagram soon (~ 1 hr) after cooling the mixtures into the grey areas. The N_F phase has an enantiotropic (*T*,*c*) r)egion as indicated in Fig. S8. A typical pair of DSC scans is shown in Fig. S9.

components agree well with the published values [3,6]. Upon cooling the mixtures, we observed three different liquid crystal phases: paraelectric nematic (N); antiferroelectric smectic Z (SmZ_A); and ferroelectric nematic (N_F). We refer to the N phase as 'paraelectric' using the standard condensed matter terminology for the disordered phase above a ferroelectric or antiferroelectric. At the lowest temperatures, we observed crystal phases, but their properties and composition were not investigated. The Iso, N, and N_F phases appeared in continuous fashion across the entire phase diagram, indicating complete miscibility of the two components at all concentrations in these phases. According to the miscibility rule [13], this observation answers the question posed above, indicating that the Iso, N, and N_F phases in RM734 are the same phases as in DIO. The phase range of the SmZ_A (denoted M2 in [6]), about 15°C in neat DIO, is reduced with decreasing DIO concentration, disappearing below $c \sim 50$ wt%. As is evident from Figure 2, the phase boundary into the N_F is sloped and linear in *c*, suggesting ideal mixing behaviour at this transition, as discussed in detail below.

Phase properties of note can be summarised as follows.

- *Isotropic Phase (Iso)* – The Iso phase shows extinction of transmitted light between crossed polariser and analyser and exhibits no detectable response to applied fields of up to 100 V/mm.

- *Paraelectric Nematic Phase (N)* – As expected, the N phase adopts planar alignment with a uniform, in-plane director field, $\boldsymbol{n}(\boldsymbol{r})$, parallel to the buffing direction. Excellent extinction is achieved when the cell is oriented with the director parallel to the polariser or analyser (Figure 4(a), S3B). Freedericksz transitions, driven by a 200 Hz square-wave field, were observed in the N phase (Fig. S3C), with in-plane fields generating a twist deformation of the director [RMS threshold voltage

$V_{th}^{T} = 2\pi(D/d)\sqrt{K_T/(\varepsilon_0\Delta\varepsilon)}$], and fields normal to the cell plates generating splay-bend deformation [RMS threshold voltage $V_{th}^{S} = 2\pi\sqrt{K_S/(\varepsilon_0\Delta\varepsilon)}$] [23], where D is the in-plane electrode gap, K_T and K_S are the twist and splay Frank elastic constants, and $\Delta\varepsilon$ is the low-frequency dielectric anisotropy. The temperature dependence of the threshold voltages in RM734 and DIO is shown in Fig. S4. RM734 and DIO exhibit typical Freedericksz-like, thresholded orientational response to an applied field. Both RM734 and DIO exhibit a general increase in $\Delta\varepsilon$ on cooling. In RM734, however, the Freedericksz thresholds are lower and decrease on approaching the transition to the N_F phase due to the strong pretransitional growth of $\Delta\varepsilon$ and decrease of K_S [4,5], phenomena which do not occur in the N phase of DIO because in this material the nematic approaches an antiferroelectric phase on cooling. The observed splay threshold voltage of RM734 agrees well with V_{th}^{S} calculated using the K_S and $\Delta\varepsilon$ values given in Refs. [4,5]. Comparison of the measurements with the theoretical twist/splay threshold ratio enables an estimate of the elastic constant ratio K_T/K_S. The dashed lines in Fig. S4 give V_{th}^{S} scaled up by 286, showing that $K_S > K_T$ in both materials, except near the N–N_F transition in RM734, due to the pretransitional decrease of K_S [4,5]. In DIO, K_S ~10 K_T over most of the nematic range.

- *Lamellar Antiferroelectric LC with In-Plane Nematic Director (SmZ_A)* – We have recently determined, using non-resonant SAXS on magnetically aligned capillaries and PLM electro-optic measurements of aligned cells, that the previously reported [6] but structurally uncharacterised M2 phase of DIO is a layered (density-modulated), antiferroelectric LC, which we name the smectic Z_A (SmZ_A), comprising a periodic array of 9 nm thick, polar layers with alternating polarisation and a nematic director parallel to the layer planes [14]. In cells, these layers fill three-dimensional space in well-defined, smectic-like geometries, with the layers either parallel or normal to the plates. Upon cooling from the N phase in a cell with buffed polyimide surfaces, the layers grow in normal to the plates, suppressing the in-plane twist Freedericksz response to fields applied in the plane of the cell but preserving the splay-bend Freedericksz transition for fields applied normal to the plates. These features make it easy to distinguish the SmZ_A from both the N and N_F phases.

- *Ferroelectric Nematic Phase (N_F)* – The textural evolution of the N_F phase obtained on cooling a uniform domain of the SmZ_A phase in neat DIO is shown in the PLM images of Figure 3 (a-d), and that on cooling a uniform domain of the N phase in the $c = 40$ wt% DIO mixture in Figure 4, both in the absence of field. In addition to undergoing characteristic optical changes, the transition to the N_F is marked by an increase in the threshold for the splay-bend Freedericksz transition, from a few tenths of a volt in the N phase to more than 100 V in the N_F phase, a result of the large electrostatic energy cost of rotating the ferroelectric polarisation $\boldsymbol{P}$ in an initially planar cell to give a component normal to the cell plates [7]. At the same time, the threshold field for in-plane field-induced twist is reduced by about a factor of 1000 because of the development of ferroelectric coupling between $\boldsymbol{P}$ and $\boldsymbol{E}$ [7], giving extreme electro-optic responsivity to very weak applied in-plane electric fields (in the 0.1 to 1 V/mm range) in all of the N_F director states shown. At the N to N_F transition, a front characterised by local orientation fluctuations passes through the cell (Figure 4(b)), leaving behind a smooth, planar texture in the N_F phase, retaining the uniform director field of the N (and SmZ_A) phases with $\boldsymbol{n}$ parallel to the buffing axis (the U state) for several degrees into the N_F phase. On further cooling, however, a structural transition occurs, with distinct transition lines (π-twist disclination lines formed at one surface) passing laterally across the cell and mediating the formation of left- and right-handed (*LH* and *RH*) π-twist domains, which are non-extinguishing and are themselves separated by another kind of distinct line defect (2π-twist lines in the cell midplane), seen in Figures 3(a) and 4(c). These twisted states appear optically identical between crossed polariser and analyser, but their equivalence is lost when the polarisers are decrossed, with the *LH* and *RH* domains exhibiting distinct colours that are exchanged when the polarisers are decrossed the other way (Figure 3(b-d)). This behaviour, first observed

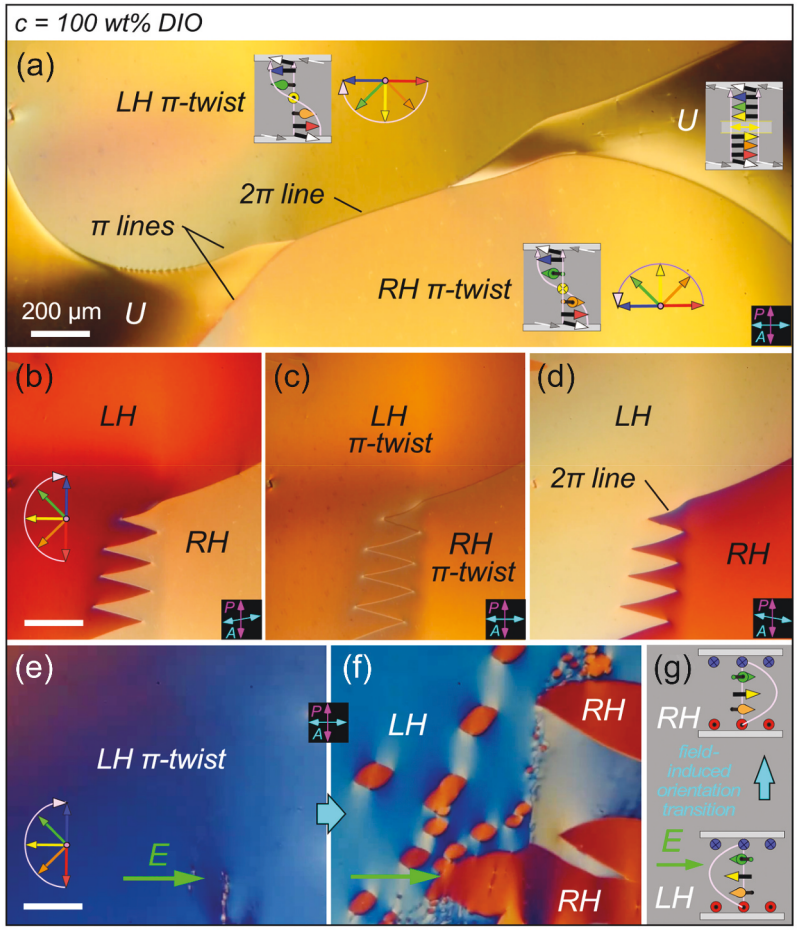

Figure 3. (Colour online) Domain evolution and field response in the N_F phase of neat DIO. This cell is $d = 3.5$ μm thick and has antiparallel, unidirectional buffing on the two plates, favouring twisted director states. Scale bar is indicated in (a). (a) The initial director state observed on cooling into the N_F phase is initially uniform-planar (*U*), like the N and SmZ_A phases, but upon cooling a few degrees further (to $T = 65$°C), left- and right-handed π-twist states preferred by the polar surfaces develop. The boundary between domains with opposite twist is a 2π-twist disclination line. Red-to-blue arrow sequences represent the ferroelectric polarization orientation at increasing heights in the cell ($x = 0$, $d/4$, $d/2$, $3d/4$, d), with pink arrows indicating the progression of the polar azimuth φ (x) from the bottom to the top of the cell, which is also the light propagation direction. The initial optically uniform (*U*) state sketched at right, which has a localised polarisation reversal wall in the interior of the cell, transitions to a continuous π-twist state by passage of a π-twist surface line. While the uniform state can be extinguished between crossed polariser and analyser, the twist state remains birefringent independent of sample orientation. (b-d) Decrossing the analyser lifts the optical degeneracy of the *LH* and *RH* states, giving distinct colours that reveal their underlying chirality. Reversing the decrossing angle causes the two twisted states to exchange colours, showing that their director structures are mirror symmetric [15]. (e-g) Twist reversal in an applied field. In the relaxed π-twist states, the N_F polarisation at mid-height in the cell points in opposite directions in the *LH* and *RH* regions. Since the buffing in this cell is parallel to the electrode edges, an applied electric field of a particular sign favours either the *LH* or the *RH* state and can therefore be used to drive the cell between these two configurations by nucleation and growth of the preferred state. In this example, the field favors the *RH* twist state. The scale is the same in all images.

in *ANTIPOLAR* cells of neat RM734 [15], indicates a spontaneous transformation of the uniform nematic director/polarisation state into a π-twisted state by passage of a π-twist line. This observation is critical and unambiguous confirmative evidence for nematic ferroelectricity: a spontaneous uniform to π-twisted transition in an antiparallel-buffed cell in the N_F phase is a uniquely ferroelectric nematic phenomenon, requiring not only macroscopic polar ordering of the bulk LC but also polar coupling to a macroscopically polar surface. The *LH* and *RH* π-twist states support, respectively, a half-turn of a left- or right-handed

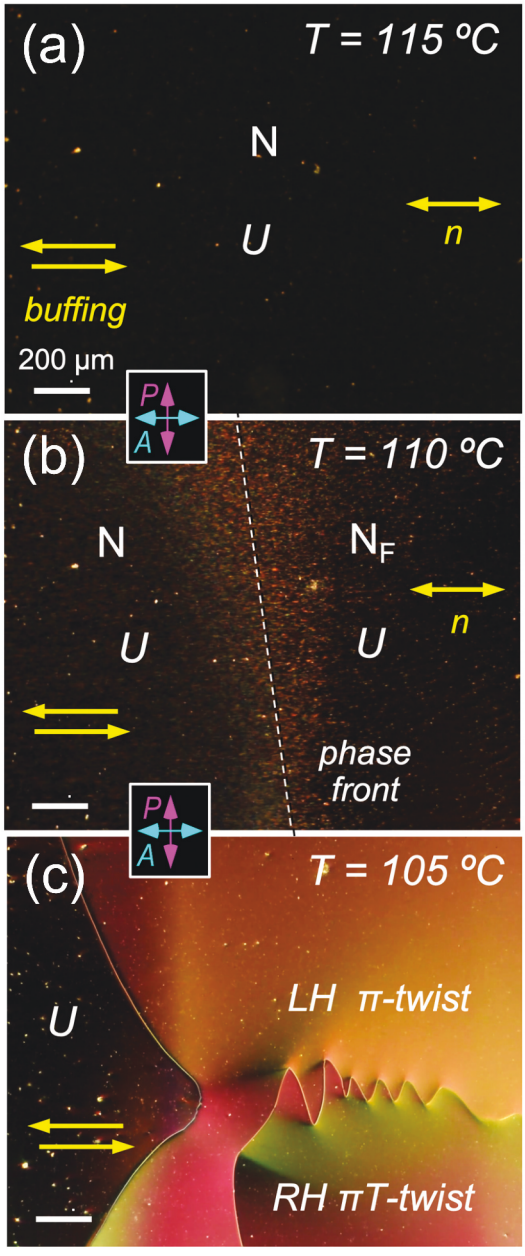

Figure 4. (Colour online) Textural changes observed on cooling a $c = 40$ wt% DIO mixture through the N – N_F transition in a $d = 3.5$ µm cell with antiparallel, unidirectionally buffed surfaces. (A) In the N phase, the director field is uniform (*U*) and along the buffing direction. (b) This condition is initially retained in the N_F, once the phase front (dashed white line), characterised by the temporary appearance of irregular, polar domains extended along the director, passes through the cell. (c) With a few degrees of additional cooling in the N_F phase, π-twist states stabilised by the increasingly strong antipolar surface anchoring nucleate and grow in the previously uniform N_F region. Color variations within the twisted regions result from the coupling of the $\boldsymbol{n}(r)/\boldsymbol{P}(r)$ couple over the area of the domains to in-plane electric fields generated by polarization charge on the twist walls. Such twisted states are observed in DIO mixtures of all concentrations. Interestingly, spontaneous periodic modulations of the director like those reported in the N_F phase of neat RM734 [5] are not observed in any of the mixtures or in neat DIO.

director helix and are separated by topological 2π-twist lines. The two twist states have opposite net polarisation, normal to the buffing axis, so that reversing an electric field applied in this direction can be used to switch between them, as shown in Figure 3(e-g). Such π-twist states are observed in all of the mixtures and in neat DIO, and show behaviour qualitatively similar to that observed in neat RM734 [7,15], leading us to conclude that the N_F is continuous across the phase diagram. Li et al. have also noted similarities in RM734 and DIO textures observed in random-planar cells [8].

Transition to the N_F Phase

This transition is distinctly different at the two ends of the phase diagram. In RM734-rich mixtures, upon approaching the N – N_F transition, we observe a random pattern of fluctuating polar domains, as previously reported in neat RM734 [4,7] and shown in Figure 4(b). These domains are extended along the director orientation, $\boldsymbol{n}$, in a manifestation of the electrostatic suppression of longitudinal fluctuations of the polarisation $\boldsymbol{P}$ [7]. The details of coarsening of these domains upon cooling into the N_F depends on the surface conditions, but in few-micron thick, rubbed polyimide cells the domains typically grow to several microns in size, eliminating defects in the texture and forming large, uniform monodomain and then twisted states [15]. In thicker or more weakly aligned cells, the length scale of the coarsening domains has been observed to increase continuously on cooling to millimetre dimensions [24], with irregular, macroscopic patterns of reversed polarisation extended along the director, as seen in RM734 [7,8,11,24] and in a homolog of DIO that transitions directly from N to N_F [8]. In typical test cells, the uniform N_F domains are separated either by pure polarisation reversal walls or by splay-bend walls [7,8]. This behaviour, along with the ferroelectric uniform and twisted states observed in DIO, suggest that the N_F phase observed in the mixtures is the same as that in RM734 and DIO.

We note that we have not observed periodic birefringent (splay nematic) stripes with ~9 µm spacing of the kind previously reported in the N_F phase of the RM734 family by Mandle and co-workers [5,11] in the N_F phase of any preparations of RM734, DIO or their mixtures, in any standard thin cells, capillaries, or thicker (10–50 µm) cells with planar or random-planar alignment.

At the DIO end of the phase diagram, the transition sequence on cooling is first N – SmZ_A and then SmZ_A – N_F. These transitions are weakly first-order, and the phases grow in as optically distinct, uniform domains upon cooling, without the dramatic polar fluctuations seen at the N – N_F transition. We attribute this to the antiferroelectric ordering of the SmZ_A phase. Over most of the SmZ_A phase, in-plane reorientation of the director field is strongly suppressed but at lower temperatures, approaching the transition to the N_F phase, ferroelectric fluctuations appear and the susceptibility for field-induced reorientation increases, to be discussed in a later publication.

Ferroelectric Polarisation

A typical set of polarization current, $i(t)$, vs. time measurements in response to a 50 Hz, 104 V/mm square-wave, in-plane applied field at different temperatures, in this case for the $c = 90$ wt% DIO mixture, is plotted in Figure 5(a), with additional data included in Fig. S5. This weak applied field is large enough to reverse the polarisation in the N_F. In the Iso, N and SmZ_A phases, the current consists only of a signal that peaks shortly after sign reversal of the applied voltage and then decays exponentially. This signal corresponds to the RC-circuit linear response of the cell and series resistance, giving the initial upward curvature of the measured P, due to increasing ε in the N phase as the N_F phase transition is approached. At the transition to the N_F, a much larger current signal, resulting from the reversal of spontaneous polarisation in the sample, appears at longer times. This current peak is integrated in time to obtain the net charge flow $Q = \int i(t)dt$ and the corresponding charge density $Q/2A$, shown in Figure 5(b)and Fig. S5, where A is the cross-section of the liquid crystal sample in the plane normal to the applied field midway between the two electrodes.

Initial qualitative observations showed that the width in time of the current peak increased dramatically with decreasing T (Fig. S5), motivating the choice of square-wave driving in order to minimise the temporal width of the current response. Thus, at high temperatures, polarisation reversal is completed during the available 10 msec integration time between applied field reversals. In this regime, denoted by the filled square symbols in Figure 5(b), the quantity $Q/2A$ is equivalent to the bulk N_F polarisation, with $P(c,T) = Q(c,T)/2A$. We find that in this temperature range, the dependence of $P(T)$ on temperature is quite similar in all of the mixtures: on approaching the transition to the N_F phase, the polarisation increases sigmoidally, with an initial upward curvature reflecting the pre-transitional increase in dielectric constant in the N (or SmZ_A) phase observed in both RM734 [4,5] and DIO [6,8].

However, as Figure 5(a,c) show, the full width at half-maximum of the current peak associated with polarisation reversal, τ_R, increases rapidly on cooling. Below a temperature T_{sat}, even with square wave driving, polarisation reversal cannot be completed within the available 10 msec time window and the measured $Q(c,T)/2A$ values decrease rapidly with decreasing T from their maximum value of P_{sat} (solid circles in Figure 5(b)). Test experiments with longer integration times confirm that these data do not reflect the true polarisation, which increases by a few percent above $P_{sat}(c)$ as T is lowered, as observed in RM734 and confirmed in atomistic simulations of RM734 [7]. In the following analysis of the time reversal dynamics, we approximate the polarisation at temperatures below T_{sat} simply by $P_{sat}(c)$. Under this assumption, the time reversal dynamics can be used to obtain measurement of the orientational viscosity at temperatures $T < T_{sat}$.

The saturation value of the polarisation is similar in all of the mixtures, P_{sat} ~6 μC/cm^2, as seen in Figure 5(b), with $P_{sat}(c)$ decreasing slightly from the RM734-rich to the DIO-rich end, as shown in Figure 5(d).

At low temperatures, the polarisation measurements were made approximately 30 min apart to allow time for possible crystallisation. The inset in Figure 5(a) shows the current response following field reversal of the $c = 90\%$ DIO mixture at the lowest temperatures. In this mixture, crystallisation occurred between the $T = 26.5$°C and $T = 25.5$°C scans, causing a precipitous drop in the integrated current, as is evident from the plot. In general, crystallisation is observed on cooling in mixtures at both ends of the phase diagram, near $c \sim 0$ and $c \sim 100\%$, as crystallisation becomes thermodynamically favourable at higher temperatures where the fluid N_F phase still has relatively low viscosity (grey Xtal regions in Figure 2). Interestingly, crystallisation is largely suppressed in the $c = 90\%$ DIO mixture while the square-wave polarisation reversal field is applied, but the sample crystallises within about 1 hour in the absence of field at $T = 25$°C. The polarisation reversal time was measured as a function of temperature for all the mixtures, with the results shown in Figure 5(c).

For $T < T_{sat}$, the measured $Q(T)$ data, although not giving the full polarisation, can be used to provide an upper bound estimate $f(T) = (Q(T)/2A)/P_{sat}(c)$ of the fraction of the polarisation that has

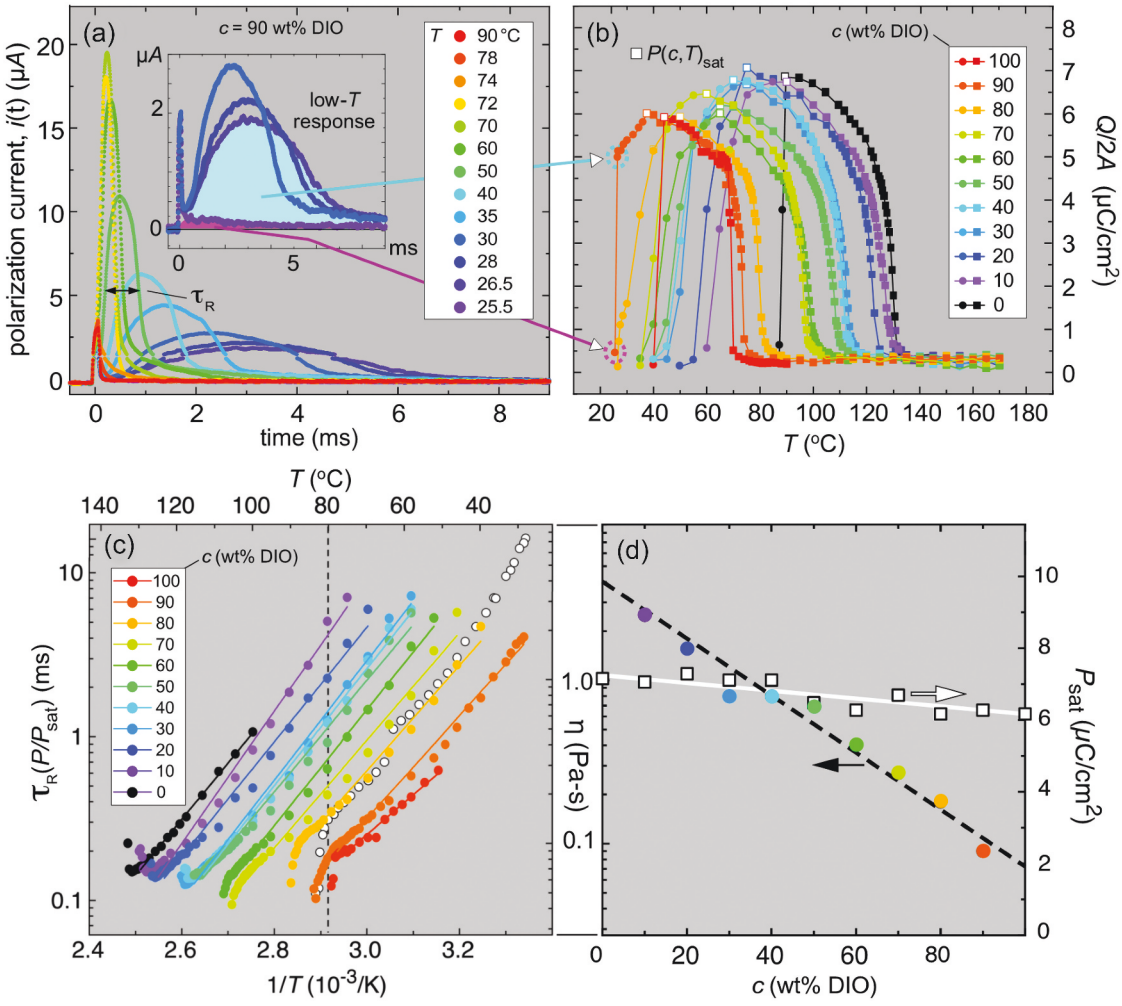

Figure 5. (Colour online) Characteristics of polarisation reversal in DIO/RM734 mixtures. A 50 Hz square wave with a peak amplitude of 104 V, applied to ITO electrodes with a 1 mm gap in a $d = 8$ μm thick, planar-aligned, cell, results in an in-plane field of 69 V/mm in the centre of the gap. This relatively small field is large enough to achieve full reversal of the bulk polarisation in the N_F phase at higher temperatures. The polarisation is determined by integrating the current through the cell over one half-cycle of the driving voltage (10 msec). (a) Polarization current vs time for the $c = 90$ wt% DIO mixture as a function of temperature. The inset shows the current response at the lowest temperatures. The small current peak seen in the N phase (at T = 90 °C) is the capacitive response of the cell to the driving voltage. Upon cooling through the $SmZ_A - N_F$ transition, a large polarisation reversal current peak develops, peaking at around $T = 70$°C before becoming smaller and broader on further cooling due to the increasing viscosity. The polarisation reversal time, τ_R, is taken as the full width of the current peak at half-maximum. The inset shows the response at low temperatures. At $T =$ 26.5°C the sample still switches ($\tau_R = \sim 6$ msec) but on cooling to $T = 25.5$°C polarisation reversal is prevented by crystallisation. (b) Integrated charge/area, $Q/2A$, transported during field reversal in neat RM734 and DIO and their mixtures. For $T > T_{sat}$ (solid squares), complete switching of P takes place between each field reversal and $Q/2A$ corresponds to the ferroelectric polarisation $P(c,T)$. The maximum polarisation, $P_{sat}(c)$, indicated with white squares here and in (d), is measured at a temperature T_{sat}, below which the director reorientation slows down and the polarisation reversal is incomplete (solid circles), so that Q reflects only part of the true polarisation density ($Q < 2AP$), which, based on computer simulations and additional measurements, increases weakly from $P_{sat}(c)$ as T is decreased from T_{sat}. (c) Plot of polarisation reversal dissipation coefficient values, $\eta(c,T) = 0.1[P(c,T)\tau_R(c,T)]E$, vs. inverse temperature: (left scale) $\tau_R(T)$ scaled as $\tau_R(T)P(T)/P_{sat}$, proportional to $\eta(c,T)$; (right scale) $\eta(c,T)$. Reversal times were evaluated only at higher temperatures ($T > T_{sat}$), where reorientation was completed between field reversals. The dissipation shows an Arrhenius-like dependence on temperature. The switching times of the three-component DIO/RM734/W1027 mixture described in the text are plotted as white circles. These were measured at low temperature using a longer integration time. (d) Polarization reversal dissipation coefficient variation with concentration (coloured circles) at fixed temperature [$T = 80$°C, dashed black line in (c)]. The dissipation coefficients of the two components are seen to add logarithmically in the mixtures. The saturation polarisation $P_{sat}(c)$ (white squares) varies approximately linearly across the phase diagram, indicating ideal mixing in the thermodynamics of the transition to the N_F phase.

reoriented within the 10 msec integration window, under the assumption that for $T < T_{sat}$, $P(c,T) = P_{sat}(c)$. The precipitous reduction in the measured charge density at the lowest temperatures coincides with a sudden increase in switching time, which results from a rapid rise in the effective orientational viscosity on approaching the glassy state. In the middle range of concentrations, there is no evidence of crystallisation, which is impeded at low T by the high viscosity and by freezing-point depression, with cooling resulting instead in a glassy state. Crystallisation could be suppressed at all DIO concentrations by rapid cooling, enabling any mixture to be quenched into a room-temperature glass.

Polarisation reorientation dynamics: orientational viscosity measurement

The characteristic time for electric fielddriven polarisation rotation (ROT) in the N_F phase is $\tau = \gamma_1/PE$, the intrinsic response time for an induced 90° rotation starting from the high-torque situation where $\boldsymbol{P}$ is normal to $\boldsymbol{E}$ [15]. This E-field-induced director reorientation process is analogous to that occurring when a magnetic field rotating with frequency ω is applied to a nematic, in which case the net local torque applied to the fluid is the same everywhere, resulting in no fluid motion, and the orientational drag is simply $\gamma_1\omega$, where γ_1 is the principal 'nematic rotational viscosity' [23]. $\tau(E)$ was measured optically in the N_F phase of RM734 and found in 90° ROT dynamics to scale as $1/E$, as expected from this picture. The optical response probes $\varphi_E(t)$, the orientation of a uniform polarisation field, and γ_1/PE is measured using the equation of motion $\varphi_E(t) = 2\tan^{-1}[\tan(\varphi_o/2)\exp(-tPE/\gamma_1)]$, where φ_o is the starting angle between $\boldsymbol{P}$ and $\boldsymbol{E}$. This enables a direct measurement of the orientational viscosity γ_1 [15].

The polarisation reversal process is in general much more complex, involving flow, domain growth and the motion of domain walls. However, in RM734 we noticed previously that, in spite of this complexity, the response time τ_R in the polarisation measurement cell with a 1 mm electrode gap also scaled as $1/E$, with $\tau_R \approx 10\tau = 10\gamma_1/PE$ [15]. Polarisation reversal takes this long because $\boldsymbol{P}$ is generally oriented antiparallel to $\boldsymbol{E}$ immediately after the field is reversed, at a very low-torque orientation through most of the cell volume. We used the same 1 mm-gap cell geometry and voltage waveform to obtain the polarisation REV data for DIO shown in Figure 5. Assuming that the same scaling relation $\tau_R \sim 10\tau$ applies in DIO, we can extract the effective ferroelectric nematic polarisation reversal dissipation coefficient, $\eta(c,T)$, from the $\tau_R(c,T)$ data as $\eta(c,T) = 0.1[P(c,T)\tau_R(c,T)]E$. $\eta(c,T)$ also has units of viscosity: torque per unit volume (N/m^2)/reorientation rate (sec^{-1}).

The measured polarisation reversal dissipation coefficient of all of the mixtures is $\eta \sim 0.05$ Pa·s at the highest temperatures in the N_F phase, increasing on cooling to $\eta \sim 3$ Pa·s at the longest measurable times (when τ_R reaches 10 msec). The dissipation coefficient of each mixture shows a nearly Arrhenius-type dependence on temperature (Figure 5(c)), suggestive of a barrier-limited dissipation process. The experimental data do generally exhibit upward curvature, trending above the Arrhenius line at the lowest temperatures, which we attribute to the approach to a transition to a glassy state. An onset temperature, $T_g(c)$, taken to be where the measured polarisation has dropped to 80% of P_{sat} ($f(T) = 0.8$), which is coincidentally also where $\tau_R \sim 5$ msec, is shown as open triangles in Figure 2. This transition temperature varies nearly linearly with concentration, paralleling that of the T_{NF} transition.

Room temperature ternary mixture

The low-temperature dynamics of the $c = 90$ wt% DIO mixture, whose N_F phase persists to room temperature, were explored further by mixing in a third component, W1027 (shown in Fig. S2), to make a (70 wt% DIO)/(15 wt% RM734)/(15 wt% W1027) mixture. Samples of this mixture formed a room temperature, fluid N_F phase that was stable against crystallisation for many hours. The temperature dependence of the viscosity of this mixture is plotted as white circles in Figure 5(c).

Phase behavior

In the case of DIO/RM734, we observe binary mixtures that exhibit a first-order transition between two phases that span the phase diagram across all DIO concentrations c. Such mixtures are considered 'ideal' if, in the calculation of the phase boundary temperature $T(c)$, the entropy of mixing is the only specifically mixing-related thermodynamic contribution that needs to be considered, besides a linear weighting of the transition enthalpy (ΔH) and entropy (ΔS) change of the individual components, based on their mole fraction. This is to say that 'excess' contributions to the difference of Gibbs potential between the two phases, ΔG, are negligible. Such contributions would appear in an A/B mixture, for example, if there were attraction, repulsion, disordering, or ordering in A-B molecular pairing that differed from the simple averaging of these effects in A-A and B-B pairing. Under conditions of ideal phase

behaviour, $T_{NF}(c)$, the centre temperature of the phase coexistence range at the transition to the N_F phase, is described by the Schroeder – van Laar (SvL) equations [25,26]:

$$T_{NF}(x) = \frac{\Delta H_{ave}(x)}{\Delta S_{ave}(x)} = \frac{xT_{DIO}\Delta S_{DIO} + (1-x)T_{RM734}\Delta S_{RM734}}{x\Delta S_{DIO} + (1-x)\Delta S_{RM734}}$$

where x = mole fraction, $T_{DIO} = 343$K and $T_{RM734} = 405$K are the neat DIO and RM734 transition temperatures to the N_F, and $\Delta S_{DIO} = 0.07R$ [6], $\Delta S_{RM734} = 0.06R$ [9], $\Delta H_{DIO} = 0.2$ kJ/mol [6], and $\Delta H_{RM734} = 0.2$ kJ/mol [9] are the per-mole quantities of the pure components. This theoretical SvL phase boundary is generally curved in the x,T plane, but is confined in temperature to the range $T_{DIO} < T(x) < T_{RM734}$. Under ideal mixing conditions, $\Delta S(x)$ should linearly interpolate between these limits. Inspection shows that if $\Delta S_{DIO} = \Delta S_{RM734}$, then the condition observed in the RM734/DIO mixtures is obtained: $\Delta S(x)$ is constant and is eliminated from the equation, with $T(x)$ becoming a linear function of x, and the phase boundary forming a straight line between T_{DIO} and T_{RM734} across the phase diagram in x, and an almost straight line in c because of the small difference in molecular weights ($MW_{RM734} = 423$, $MW_{DIO} = 510$). DSC measurement of $\Delta S(x)$ at the intermediate concentrations gives $\langle \Delta S(x) \rangle = 0.056 \pm 0.02\ R$, comparable to the values of ΔS_{DIO} and ΔS_{RM734} given above.

At the RM734 end of the phase diagram, the N – N_F transition is direct and first-order, whereas at the DIO end, the phase sequence involves two first-order transitions: N – SmZ_A – N_F. However, the linear variation of $T(x)$ vs. x is maintained irrespective of whether the transition into the N_F is from the N or the SmZ_A phase. Since $T(x)$ is governed by the intersection of the Gibbs free energy surfaces governing the N – N_F transition, which linearly interpolate between those of the pure components, the linearity of $T(x)$ suggests that the thermodynamic effect of the N – SmZ_A transition is minor. This is likely a consequence of the extremely small N – SmZ_A transition enthalpy ($\Delta H_{NZ} = 0.003$ kJ/mol [8]), and is also consistent with the $\langle P = 0 \rangle$ nature of both the paranematic N and antiferroelectric SmZ_A phases: all of the net polarisation of the N_F phase is developed through the final transition to the N_F, at the phase boundary marked with magenta dots in Figure 2. The small ΔH_{NZ}, the linearity of the dependence of $T_{NF}(c)$ vs. c, and the similarity across the phase diagram of the transition entropy of the final transition to the N_F are consistent with the $P(T,c)$ curves having comparable saturation values.

The current proposed models for the phase change from the quadrupolar but non-polar N phase to the quadrupolar and polar N_F phase are that it is either a first-order Landau-de Gennes mean-field transition [4,5], or an Ising-like orientational transition of molecular dipoles having a binary choice of orientations (along $+\boldsymbol{n}$ or $-\boldsymbol{n}$), made first-order by long-range dipole-dipole interactions [7]. In both cases, the polarisation $P(T)$ is the principal order parameter of the transition. Figure 5(b) shows that the growth of $P(T)$ is similar for the different concentrations, and Figure 5(d) that $P_{sat}(c)$ has a weak linear dependence on c. In the context of ideal mixing, this observation constrains the dependence on c of the parameters in such theories of the transition. In the Ising-like system, for example, since T_{DIO} is somewhat smaller than T_{RM734}, the Ising interaction energy $J_{ij}(x)$, which gives the local ferroelectric interaction between pairs of dipoles (i,j = DIO,DIO; i = DIO, j = RM734; i,j = RM734,RM734), and which is proportional to $T(x)$, must linearly interpolate like $T_{NF}(x)$. This happens only if $J_{DR} = (J_{DD} + J_{RR})/2$, for which condition ΔG will have no 'excess' internal energy. For the nearest-neighbour Ising model (giving a second-order phase transition in 3D), the entropy is a universal function of T/J, in which case there will also be no 'excess' entropy contribution to ΔG.

However, the transition to the N_F has been found to be first-order and mean-field-like [4,5], and to exhibit highly anisotropic orientational correlations in the N phase [7], features which can be understood with a model that includes the effects of the long-range dipole-dipole interactions on the fluctuations in the N phase. The critical behaviour of Ising systems with long-range interactions has been studied extensively in the context of certain magnetic materials that have short-range ferromagnetic exchange forces, but where the long-range dipolar interactions are also important [27–29]. Renormalisation group analysis shows that the long-range interactions make the magnetic correlations dipolar-anisotropic near the transition in the high-temperature phase [30,31], as observed in RM734 [4,7], extending them along $\boldsymbol{n}$, the $\boldsymbol{z}$ axis, by strongly suppressing longitudinal charge-density fluctuations, $\partial Pz/\partial z$ [27,28]. Specifically, starting with the free energy expression Eq. (1) from [5] and adding a dipole–dipole interaction term [7], the structure factor for Ornstein-Zernicke polarisation fluctuations of P_z about $q = 0$ becomes $\langle P_z(\boldsymbol{q})P_z(\boldsymbol{q})^* \rangle = k_B T\chi(\boldsymbol{q})$, with $\chi(\boldsymbol{q}) = 1/[\tau(T)(1$

$+ \xi(T)^2q^2) + (2\pi/\varepsilon)(q_z/q)^2]$. Here, the correlation length $\xi(T)^2 = b/\tau(T)$, $\tau(T) \propto (T\text{-}T_{NF})/T_{NF}$, b is a constant, and $\boldsymbol{q} = \boldsymbol{q}_z + \boldsymbol{q}_y$. The dipole-dipole (third) term produces extended correlations that grow as $\xi(\tau)$ along x and y but as $\xi(\tau)^2$ along z [28], suppressing $\chi(\boldsymbol{q})$ for finite q_z as is observed qualitatively from the image sequences of the textures upon passing through the phase transition, and from their optical Fourier transforms (see Fig. S9 in Ref. [7]). Because of this anisotropy, the correlation volume in this model grows in 3D as $V \sim \xi(\tau)^4$ rather than the isotropic $V \sim \xi(\tau)^3$, reducing the upper marginal dimensionality of the transition to three and making the transition mean-field-like with logarithmic corrections, rather than fluctuation-dominated with 3D Ising universality [32]. The dipole-dipole term scales as P^2, so the nearly equal dipole moments of DIO and RM734, and the nearly equal Js, would tend to make this behaviour similar across the phase diagram. Assuming for the moment that $T_{DIO} = T_{RM734}$, and therefore that $J_{DD} = J_{RR}$, the 'ideal' mixture averaging condition $J_{DR} = (J_{DD} + J_{RR})/2$ reduces to $J_{DR} = J_{DD} = J_{RR}$: the molecules behave identically with respect to their pair interaction energy, stabilising the N_F phase.

Polarisation reversal dissipation coefficients of the mixtures

The measured dissipation coefficient values, $\eta(c,T) = 0.1[P(c,T)\tau_R(c,T)]E$, were fit to the Arrhenius form $\eta(T) = A\exp[E_\eta/k_BT]$, as shown in Figure 5(c), in order to determine the effective barrier height, E_η. As can be seen from the uniformity of the slopes, E_η is essentially independent of c, with an average value of $E_\eta = 7800$K across the phase diagram. The coefficient A, in contrast, varies substantially with c, behaviour that can be quantified by measuring the viscosity vs. concentration at a single temperature, for example 80°C. The plot in Figure 5(d) shows logarithmic additivity of $\eta(T)$ for the DIO/RM734 mixture: $\ln[\eta(80°C)] = (x)\ln[\eta_{DIO}(80°C)] + (1\text{-}x)\ln[\eta_{RM734}\ (80°C)]$. A basic understanding of this behaviour can be gained by using the combined Cohen-Turnbull free volume [33]/Eyring rate theory [34] model proposed by Macedo and Litovitz [35]. This model is based on Maxwell's intuitive picture [36], or its contemporary embodiments [37,38], in which viscosity $\eta = G/\nu$, the ratio of G, a typical elastic modulus for local shear deformation, to ν, the average rate per molecule of randomly occurring, local structural deconfinement/relaxation events. The rate ν is given by $\nu = \nu_T p = \nu_T p_E p_V$, where ν_T is a trial frequency, and p the probability of success, a product of the probability $p_E = \exp(-E_\eta/E)$ that sufficient energy, E, will be available [34], and $p_V = \exp(-V/V_f)$ [33], the probability that sufficient free volume, V, will be available, where V_f is the average free volume per particle. These probabilities relate viscosity to temperature and density, respectively, giving the generalised relationship, $\eta(T) = G/(\nu_T p_E p_V) = (G/\nu_T)\ \exp(cV_o/V_f + E_\eta/k_BT)$, where V_o is the close-packed volume per particle, and the available energy is on average k_BT. Applying this to the DIO/RM734 mixtures, we can consider G and ν_T to be the same for the two components and, since the Kelvin range is rather narrow, also to be independent of temperature, with the difference in viscosity of the components being the result of a difference in V_f. Generally, in a binary mixture we will have

$$\begin{aligned}\nu = \nu_T p &= \nu_T (p_{DIO})^x\ (p_{RM734})^{1\text{-}x} \\ &= \nu_T[(p_E)_{DIO}{}^x\ (p_V)_{DIO}{}^x\ (p_E)_{RM734}{}^{1\text{-}x}\ (p_V)_{RM734}{}^{1\text{-}x}].\end{aligned}$$

This expression can be simplified by noting from the similar slopes of the $\ln\eta(T)$ vs $1/T$ fits in Figure 5(c) that we can take E_η to be the same for the two components, $(E_\eta)_{DIO} = (E_\eta)_{RM734}$, from which simplification we get $(p_E)_{DIO} = (p_E)_{RM734} = p_E = \exp(-E_\eta/k_BT)$. The viscosity of the mixture is then given by $\eta(x,T) = (G/\nu_T)[p_E{}^x p_E{}^{1\text{-}x}\ (p_V)_{DIO}{}^x\ (p_V)_{DIO}{}^{1\text{-}x}]^{-1} = \eta_{DIO}(T)^{\ x}\ \eta_{RM734}(T)^{\ 1\text{-}x}$, which predicts logarithmic additivity of the viscosities, behaviour that is evident from the experimental data plotted in Figure 5(d). In the context of the model above, given that $(E_\eta)_{DIO} = (E_\eta)_{RM734}$, this logarithmic additivity implies that the effective free volume in the mixtures is obtained from a linear combination of V_o/V_f for the two components.

Enantiotropic N_F and SmZ_A phases

All single-component N_F materials reported to date, including RM734 and DIO, are monotropic, with the N_F phase observed only on cooling, implying that the N_F state is thermodynamically metastable relative to the crystalline state. When held at a fixed temperature in the N_F state, such single-component materials eventually crystallise, on timescales ranging from seconds to days [8]. For practical applications of N_F materials, enantiotropic behaviour (i.e., the existence of a thermodynamically stable N_F phase) is highly desirable. Mixing of multiple components is a well-established route to achieving enantiotropic behaviour in liquid crystals, and, in fact, enantiotropic N_F behaviour has been described previously by Mandle and co-workers, in mixtures of homologs of RM734 [9]. In order to study the enantiotropic behaviour in mixtures of RM734 and DIO, samples were filled into 8 μm-thick cells in the isotropic phase and cooled to room temperature, where they were left undisturbed for two months. Of all the mixtures exhibiting a glassy state, only the 90% DIO sample showed some recrystallisation in parts of the cell after this time. The cells were then heated slowly, with no applied field, and the phase behaviour observed in

the polarised light microscope. The spontaneous polarisation was measured as a function of temperature using in-plane fields in a subsequent heating cycle. Based on these observations, we determined that the N_F phase is enantiotropic in RM734/DIO mixtures over a range of compositions from 10% to 80% DIO (Fig. S8, Table S1). In 10% DIO for example, the concentration that exhibits the broadest enantiotropic N_F temperature range, a thermodynamically stable N_F phase is observed from T = 97.5°C to 124.7°C. The SmZ_A phase, which is observed in the heating experiments over a wide range of compositions, is also enantiotropic, in contrast to neat DIO, in which the SmZ_A is monotropic.

Discussion

For the isotropic–nematic liquid crystal transition, commonalities observed in the phase behaviour for different molecular species having widely different molecular structure have stimulated and supported the notion that the essential elements of nematic liquid crystal structure and ordering could be modelled based on a few relevant molecular features. Thus, nematics were found to be dielectric and non-polar in the absence of a field, separated from the isotropic by a first-order phase transition with transition enthalpies ~1 kJ/mol, and optically uniaxial, with a birefringence that increased slowly with decreasing temperature or increasing concentration. Maier-Saupe [39] and Onsager [40] showed that anisotropic steric shape and/or van der Waals forces, employed to describe intermolecular interactions in simple mean-field or second-virial statistical mechanical models, were the molecular features required to get a basic description of nematic ordering.

The results presented in this paper suggest that a similar distillation might be possible with respect to the ferroelectric nematic phase, showing that the effects of family origin on the interactions of molecularly distinct species leading to the ferroelectric nematic phase can be accounted for by the simplest averaging procedures to get $\Delta H(T,x)$ and $\Delta S(T,x)$ This means, for example, that at low concentration of either of the components, its isolated molecules interact with the sea of the other molecular family in a fashion similar to how they interact with their own kind.

What are the required generic molecular features for nematic ferroelectricity? There are currently ~60 molecules among the two families known to induce nematic ferroelectricity, including more than 40 molecules synthesised from the two families reported in recent papers by Li et al. [8] and twenty-five variants in the RM734 family reported by Mandle et al. [11]. Figure 1 and Table S1 of [8] summarise the observed phase behaviour of the Li compounds as pure materials, dividing them into three categories: *green (9 molecules)* – exhibiting a long-lived monotropic N_F phase; *blue (12 molecules)* – exhibiting a short-lived monotropic N_F phase that was difficult to study because of rapid crystallisation; and *red* (*21 molecules)* – exhibiting no N_F phase. This impressive exploration of the effects of a variety of substitutions shows that within these families there is a general tendency to form the N_F phase.

The similar molecular-rod shape and size (~three rings long), and the similarly large molecular dipole moments (~11 Debye) in the two families, suggest that these attributes are essential to exhibiting an N_F phase. While this combination may be necessary, it is certainly not sufficient, based on: (***i***) the extensive pre-N_F literature of longitudinally polar LCs [41] which exhibit only re-entrant nematic/smectic paraelectric or antiferroelectric phases; and (***ii***) the observation that substituting -CN for -NO_2 eliminates the N_F phase in otherwise identical molecules, in spite of their comparable dipole moments [8,9]. This latter result may suggest the importance of details of the electrostatic head-to-tail self-assembly and side-by-side interaction of the resulting aggregates found in atomistic simulations [7,42]. The structure of the on-axis diffuse peaks in the WAXS patterns of RM734 and DIO exhibit common features, summarised in Figs. S6,S7. These features are unusual among nematics, and may indicate a common enhanced tendency for head-to-tail self-assembly.

Mertelj, Mandle, and co-workers have posited [4,5,10,11] that in the RM734 family, a bulky side group like MeO in the ortho-position is required to stabilise the new N_X phase, an antiferroelectric, periodic array of splay stripes, by making the molecules more pear-shaped. More recent papers [7,8,15,24], and the observations reported here, show that the textures of the N_F phase are often not macroscopically modulated or locally splayed on any observable length scale. Furthermore, some of the more recent additions to the molecular pallet that exhibit the N_F phase have side groups in the middle or on the other end of the molecule (e.g., the RM734 family compounds 2a-2c and 3 in [8]), or lack side groups altogether (e.g., many members of the DIO family, and the RM734 family compound 12 in [8], which is the same as compound 10 in [11]).

The nearly ideal mixing behaviour of the chemically dissimilar compounds DIO and RM734 is at first blush surprising but suggests that the thermodynamics of mixing in binary mixtures of these materials is dominated by electrostatic interactions

and electrostatic intermolecular association. Despite their distinct functional groups and patterns of chemical substitution, DIO and RM734 have similar dipole moments (~11 D) and charge distributions characterised by an alternation in the sign of charge along the length of the molecule, features that are strongly correlated with typical pair-association motifs (e.g., head-to-tail 'chaining' and side-by-side 'docking') observed in atomistic simulations of RM734 and related compounds [7,43]. The role of longitudinal charge density modulation in stabilising the N_F phase has also recently been addressed in theoretical work by Madhusudana [44]. We hypothesise that the near-ideal miscibility of RM734 and DIO derives from their similar molecular shape, charge distribution, and electrostatic interactions, a hypothesis that may be tested by investigating the mixing behaviour of analogs of RM734 and DIO having modified intramolecular charge distributions.

N_F materials are highly unusual polar solvents that quite generally induce polar orientational order in dipolar solute molecules, a phenomenon we term 'solvent poling'. The degree of induced polar order can be quite large, as evidenced by the ferroelectric polarisation measurements in binary mixtures of RM734 and DIO reported here, which show that an RM734 N_F host imparts nearly perfect order to DIO solute molecules in the limit of low DIO concentration (and similarly for a low concentration of RM734 solute molecules in a DIO N_F host). This solvent poling phenomenon may simply result from orientation of solute electric dipoles in the large (~10^9 V/m) local electric fields present in the N_F host, but, more generally, will depend on details of intramolecular charge distribution and molecular shape. Solvent poling is a facile route to the creation of novel functional materials with optimised materials properties. For example, materials with large second-order nonlinear optical susceptibility may be engineered by solvent poling of high-beta chromophore molecules in N_F hosts

Disclosure statement

In accordance with Taylor & Francis policy and our ethical obligations as researchers, M. A. Glaser, J. E. Maclennan, D. M. Walba, and N. A. Clark are reporting that they have a financial and business interest in a company that may be affected by the research reported in the enclosed paper. We have disclosed those interests fully to Taylor & Francis, and we have in place an approved plan for managing any potential conflicts arising from that involvement.

Funding

This work was supported by NSF Condensed Matter Physics Grants [DMR 1710711 and DMR 2005170], and by Materials Research Science and Engineering Center (MRSEC) Grant [DMR 1420736].

ORCID

Xi Chen http://orcid.org/0000-0002-8359-200X
Zhecong Zhu http://orcid.org/0000-0002-3476-432X
Mitchell J. Magrini http://orcid.org/0000-0002-5535-2244
Eva Korblova http://orcid.org/0000-0002-3818-4373
Cheol S. Park http://orcid.org/0000-0003-1507-7548
Matthew A. Glaser http://orcid.org/0000-0002-8366-5598
Joseph E. Maclennan http://orcid.org/0000-0002-3587-554X
David M. Walba http://orcid.org/0000-0002-4478-3858
Noel A. Clark http://orcid.org/0000-0001-9301-5540

References

[1] Debye P. Some results of a kinetic theory of insulators. Physikalische Zeitschrift. 1912;13:97–100.
[2] Born M. About anisotropic liquids. Attempt at a theory of liquid crystals and the Kerr electric effect in liquids. Sitzungsber Preuss Akad Wiss. 1916;30:614–650.
[3] Mandle RJ, Cowling SJ, Goodby JW. A nematic to nematic transformation exhibited by a rod-like liquid crystal. Phys Chem Chem Phys. 2017;19:11429–11435.
[4] Mertelj A, Cmok L, Sebastián N, et al. Splay nematic phase. Phys Rev X. 2018;8:041025.
[5] Sebastián N, Cmok L, Mandle RJ, et al. Ferroelectric-ferroelastic phase transition in a nematic liquid crystal. Phys Rev Lett. 2020;124:037801.
[6] Nishikawa H, Shiroshita K, Higuchi H, et al. A fluid liquid-crystal material with highly polar order. Adv Mater. 2017;29:1702354.
[7] Chen X, Korblova E, Dong D, et al. First-Principles experimental demonstration of ferroelectricity in a thermotropic nematic liquid crystal: spontaneous polar domains and striking electro-optics. PNAS. 2020;117:14021–14031.
[8] Li J, Nishikawa H, Kougo J, et al. Development of ferroelectric nematic fluids with giant-ε dielectricity and nonlinear optical properties. Sci Adv. 2021;7(17):eabf5047.
[9] Mandle RJ, Cowling SJ, Goodby JW. Rational design of rod-like liquid crystals exhibiting two nematic phases. Chem Eur J. 2017;23:14554–14562.
[10] Connor PLM, Mandle RJ. Chemically induced splay nematic phase with micron scale periodicity. Soft Matter. 2020;16:324–329.
[11] Mandle RJ, Cowling SJ, Goodby JW. Structural variants of RM734 in the design of splay nematic materials. Liq Cryst. 2021;48:1780–1790.
[12] Saha R, Nepal P, Feng C, et al., Multiple ferroelectric nematic phases of a highly polar liquid crystal compound. arXiv:2104.06520

[13] Demus D, Diele S, Grande S, et al. Polymorphism in thermotropic liquid crystals. In: Brown GH, editor. Advances in liquid crystals. Vol. 6. ISBN 0. ISBN 0-120250063. 120250063. New York: Academic Press; 1983. pp. 1–107.
[14] Chen X, Korblova E, Freychet G, et al., Antiferroelectric smectic ordering as a prelude to the ferroelectric nematic: introducing the smectic Z phase. arXiv:2112.14222 (2021).
[15] Chen X, Korblova E, Glaser MA, et al. Polar in-plane surface orientation of a ferroelectric nematic liquid crystal: polar monodomains and twisted state electro-optics. PNAS. 2021;118(22):e2104092118.
[16] Margerum JD, Van Ast CI, Myer GD, et al. Experimental methods for determining the eutectic composition of a multi-component liquid crystal mixture. Mol Cryst Liq Cryst. 1991;198:29–36.
[17] Nessim RI. Applicability of the Schroeder-van Laar relation to multi-mixtures of liquid crystals of the phenyl benzoate type. Thermochim Acta. 2000;343:1–6.
[18] Kelly SM, O'-Neill M. Liquid crystals for electro-optic applications. In: Nalwa HS, editor. Handbook of advanced electronic and photonic materials and devices. San Diego, California: Academic Press; 2001.
[19] Martinez-Miranda LJ, Kortan AR, Birgeneau RJ. Phase diagram, fluctuations, and phase transitions near the liquid-crystal nematic—smectic-A—smectic-C multicritical point. Phys Rev A. 1987;36:2372–2383.
[20] Huang TM, McCreary K, Garg S, et al. Induced smectic phases in phase diagrams of binary nematic liquid crystal mixtures. J Chem Phys. 2011;134:124508.
[21] Sugisawa S, Tabe Y. Induced smectic phases of stoichiometric liquid crystal mixtures. Soft Matter. 2016;12:3103–3109.
[22] Hardouin F, Levelut AM, Achard MF, et al. Polymorphism in polar mesogens. 1. physico-chemistry and structural aspects. J Chim Phys Phys- Chim Biol. 1983;80:53–64.
[23] Oswald P, Pieranski P. Nematic and cholesteric liquid crystals: concepts and physical properties illustrated by experiments. Boca Raton: Taylor & Francis; 2005.
[24] Sebastián N, Mandle RJ, Petelin A, et al. Electrooptics of mm-scale polar domains in the ferroelectric splay nematic phase. Liq Cryst. 2021;48:1–17.
[25] Van Hecke GR. Use of regular solution theory for calculating binary mesogenic phase diagrams exhibiting azeotrope-like behavior for liquid two-phase regions. 1. Simple minimum forming systems. J Phys Chem. 1979;83:2344–2348.
[26] Van Hecke GR. The equal G analysis. a comprehensive thermodynamics treatment for the calculation of liquid crystalline phase diagrams. J Phys Chem. 1985; 89:2058–2064.
[27] Kotzler J. Critical phenomena in dipolar magnets. J Magn Magn Mater. 1986;54–57:649–654.
[28] Als-Nielsen J. Experimental test of renormalization group theory on the uniaxial, dipolar coupled ferromagnet $LiTbF_4$. Phys Rev Lett. 1976;37:1161–1164.
[29] Als-Nielsen J, Birgeneau RJ. Mean field theory, the Ginzburg criterion, and marginal dimensionality of phase transitions. Am J Phys. 1977;45:554–560.
[30] Aharony A, Fisher ME. Critical behavior of magnets with dipolar interactions. I. Renormalization group near 4 dimensions. Phys Rev B. 1973;8: 3323–3341.
[31] Aharony A. Critical behavior of magnets with dipolar interactions. V. Uniaxial magnets in d-dimensions. Phys Rev B. 1973;8:3363–3370.
[32] Ahlers G, Kornblit A, Guggenheim HJ. Logarithmic corrections to the Landau specific heat near the Curie temperature of the dipolar Ising ferromagnet $LiTbF_4$. Phys Rev Lett. 1975;34:1227–1230.
[33] Cohen MH, Turnbull D. Molecular transport in liquids and glasses. J Chem Phys. 1959;31:1164–1169.
[34] Eyring H. The activated complex in chemical reactions. J Chem Phys. 1935;3:107–115.
[35] Macedo PB, Litovitz TA. On the relative roles of free volume and activation energy in the viscosity of liquids. J Chem Phys. 1965;42:245–256.
[36] Maxwell JC. On the dynamical theory of gases. Phil Trans Roy Soc. 1867;157:49–88.
[37] Evans DJ, Morriss GP. Statistical mechanics of nonequilibrium liquids. London: Academic Press; 1990. Chapters 2 and 4.
[38] Desgranges C, Delhommelle J. Rheology of liquid fcc metals: Equilibrium and transient-time correlation-function nonequilibrium molecular dynamics simulations. Phys Rev B. 2008;78:184202.
[39] Maier W, Saupe A. Eine einfache molekulare Theorie des nematischen kristallinflüssigen Zustandes. Z Naturforsch. 1958;A13:564–566.
[40] Onsager L. The effects of shape on the interaction of colloidal particles. Ann NY Acad Sci. 1949;51:627–659.
[41] Dąbrowski R. From the discovery of the partially bilayer smectic A phase to blue phases in polar liquid crystals. Liq Cryst. 2015;42:783–818.
[42] Mandle RJ, Sebastián N, Martinez-Perdiguero J, et al. On the molecular origins of the ferroelectric splay nematic phase. Nat Commun. 2021;12:4962.
[43] Dong D, Bedrov D, Clark NA, et al., Manuscript in preparation.
[44] Madhusudana NV. Simple molecular model for ferroelectric nematic liquid crystals exhibited by small rodlike mesogens. Phys Rev E. 2021;104:014704.